OMEGA ICF Experiments and Preparation for Direct-Drive Ignition on NIF

R. L. McCrory 1), R. E. Bahr 1), R. Betti 1), T. R. Boehly 1), T. J. B. Collins 1), R. S. Craxton 1), J. A. Delettrez 1), W. R. Donaldson 1), R. Epstein 1), J. Frenje 2), V. Yu. Glebov 1), V. N. Goncharov 1), O. V. Gotchev 1), R. Q. Gram 1), D. R. Harding 1), D. G. Hicks* 2), P. A. Jaanimagi 1), R. L. Keck 1), J. Kelly 1), J. P. Knauer 1), C. K. Li 2), S. J. Loucks 1), L. D. Lund 1), F. J. Marshall 1), P. W. McKenty 1), D. D. Meyerhofer 1), S. F. B. Morse 1), R. D. Petrasso 2), P. B. Radha 1), S. P. Regan 1), S. Roberts 1), F. Séguin 2), W. Seka 1), S. Skupsky 1), V. A. Smalyuk 1), C. Sorce 1), J. M. Soures 1), C. Stoeckl 1), R. P. J. Town 1), M. D. Wittman 1), B. Yaakobi 1), and J. D. Zuegel 1)

1) Laboratory for Laser Energetics, University of Rochester, Rochester, NY, USA
2) Plasma Science and Fusion Center, MIT, Boston, MA, USA
*Currently at Lawrence Livermore National Laboratory, Livermore, CA, USA

e-mail contact of main author: rmcc@lle.rochester.edu

Abstract. Direct-drive laser-fusion ignition experiments rely on detailed understanding and control of irradiation uniformity, the Rayleigh–Taylor instability, and target fabrication. LLE is investigating various theoretical aspects of a direct-drive NIF ignition target based on an "all-DT" design: a spherical target of ~3.4-mm diameter, 1 to 2 μm of CH wall thickness, and an ~340-μm DT-ice layer near the triple point of DT (~19 K). OMEGA experiments are designed to address the critical issues related to direct-drive laser fusion and to provide the necessary data to validate the predictive capability of LLE computer codes. The cryogenic targets to be used on OMEGA are hydrodynamically equivalent to those planned for the NIF. The current experimental studies on OMEGA address the essential components of direct-drive laser fusion: irradiation uniformity and laser imprinting, Rayleigh–Taylor growth and saturation, compressed core performance and shell–fuel mixing, laser–plasma interactions and their effect on target performance, and cryogenic target fabrication and handling.

1. Introduction

Direct-drive ignition of inertial confinement fusion (ICF) targets [1] on the National Ignition Facility (NIF) is predicted to have higher gain (20~50) than indirect drive (~15) [2]. In this paper the direct-drive inertial confinement fusion (ICF) experimental program of the University of Rochester's Laboratory for Laser Energetics (LLE) is summarized. LLE's mission is to study the physics of direct-drive ICF, through both experiments on the 60-beam, 30-kJ OMEGA laser system [3] and simulations of the direct-drive performance of NIF implosions [4].

LLE's theoretical program is investigating various aspects of a direct-drive NIF ignition target based on an "all-DT" design: a spherical target of ~3.4-mm diameter, with a 1- to 2-μm CH wall thickness, and an ~340-μm DT-ice layer near the triple point of DT (~19 K). The OMEGA experimental program addresses the critical issues related to direct-drive laser fusion and provides the necessary data to validate the predictive capability of LLE computer codes. The cryogenic targets to be used on OMEGA are hydrodynamically equivalent to those planned for the NIF. The current experimental studies on OMEGA address all of the essential components of direct-drive laser fusion: irradiation uniformity and laser imprinting, Rayleigh–Taylor growth and saturation, compressed core performance and shell–fuel mixing, laser–plasma interactions and their effect on target performance, and cryogenic target fabrication and handling.

The primary constraint on direct-drive ignition is the seeding and growth of the Rayleigh–Taylor (RT) instability [1]. The RT instability occurs in both the acceleration and deceleration phases of the target implosion. During the acceleration phase, the RT instability is seeded by the imprinting of laser nonuniformity, by target outer-surface roughness, and by feed-out of inner-surface

perturbations after shock transit through the target. Additional shell distortions are caused by variations in power among the beams. The total amplitude of these perturbations must remain less than the in-flight shell thickness. Thus, direct-drive target designs must tolerate four sources of nonuniformity to ignite and burn: (1) inner DT-ice roughness, (2) outside CH capsule finish, (3) drive asymmetry, and (4) laser imprinting.

2. NIF's Direct-Drive Target Design

LLE's base-line NIF direct-drive ignition design is based on a cryogenic DT target; it requires 1.5 MJ of laser energy and places the target on an $\alpha = 3$ isentrope (α is defined as the specific energy of the fuel divided by the Fermi-degenerate specific energy) using a continuous-pulse design. Recently, significant progress was made in understanding the sensitivity of the NIF direct-drive capsule designs to laser-pulse-shape characteristics [4].

The base-line capsules are 3.4 mm in diameter and consist of a 340-μm layer of DT ice enclosed by a 1- to 2-μm-thick plastic shell (see *FIG. 1*). The continuous laser pulse used to drive these targets (shown in *FIG. 2*) consists of two distinct temporal regions: the foot and the main drive.

The laser pulse creates two main shocks in the DT-ice layer: the first is launched at the start of the pulse; the second is generated during the rise to the main drive intensity. The DT-ice thickness and adiabat of the implosion determine the length and intensity of the foot. At a foot-pulse intensity of ~10 TW, a 10-Mbar shock is launched through the DT ice. At the time of shock breakout at the rear surface of the DT ice, the pulse ramps up to the drive region, which lasts for 2.5 ns at a power of ~450 TW. This rapid rise in intensity generates pressures of approximately 80 Mbar and accelerates the DT ice inward. The highest gains are obtained when the second shock arrives at the DT-ice inner surface just shortly after the first shock.

The base-line point design is predicted, by 1-D calculations, to attain a gain of 45, a neutron-averaged ion temperature of 30 keV, and a peak ρR of ~1.3 g/cm^2. The peak in-flight aspect ratio (IFAR) of this design is 60, and the convergence ratio (initial target radius divided by the radius of the hot spot) is 28. The equation of state of the material, the ice thickness, and the laser power determine the optimum timing of the two shocks.

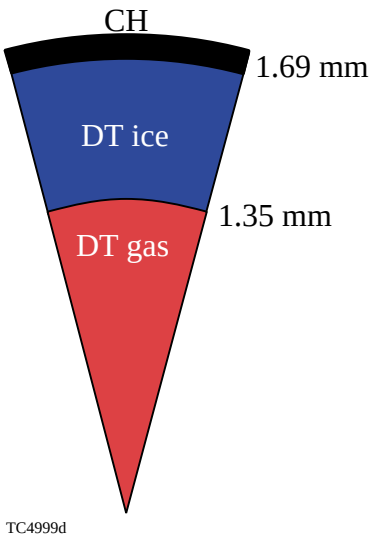

FIG. 1. *Schematic of the NIF "all-DT," direct-drive target design.*

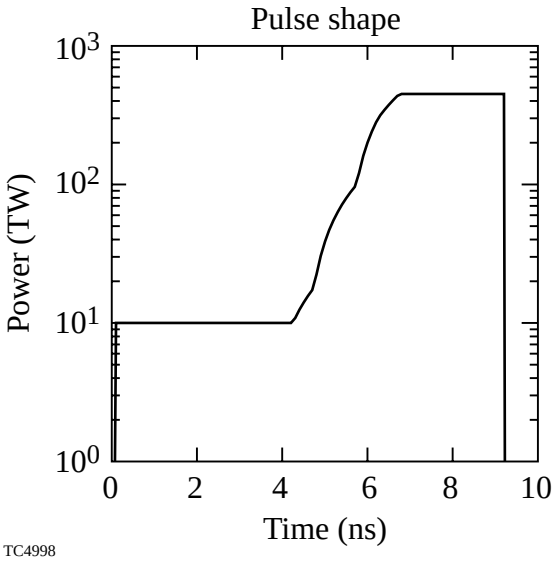

FIG. 2. *Pulse shape for the NIF direct-drive ignition target.*

Changing the length or intensity of the foot of the laser pulse controls the shock timing. A series of 1-D calculations were carried out to establish the sensitivity of the target performance to the duration and intensity of the foot. These simulations are summarized in *FIG. 3*. The gain drops when the power of the foot pulse or its duration is changed from optimum conditions. Such changes lead to a decompression of the inner part of the DT ice prior to the arrival of the second shock or to the coalescence of the two shocks prior to reaching the inner DT-ice surface. Optimal timing between the two shocks can be maintained by trading the power of the foot with its duration. For foot-pulse duration between 3.5 ns and 6 ns, the gain increases from about 40 to a maximum value of 50. The isentrope parameter α varies from 3.5 to 2.5 over that range. The design point at $\alpha = 3$ corresponds to a foot-pulse duration of 4.4 ns and a foot power of 9.5 TW, resulting in a gain of ~45 (black dot in *FIG. 3*). The black contour line in *FIG. 3* indicates the 90% gain contour around the design point and demonstrates acceptable tolerances on the foot power (±10%) and in the foot-pulse duration (±350 ps). For longer foot pulses, the gain is higher, but the isentrope is reduced, increasing the effect of the RT instability.

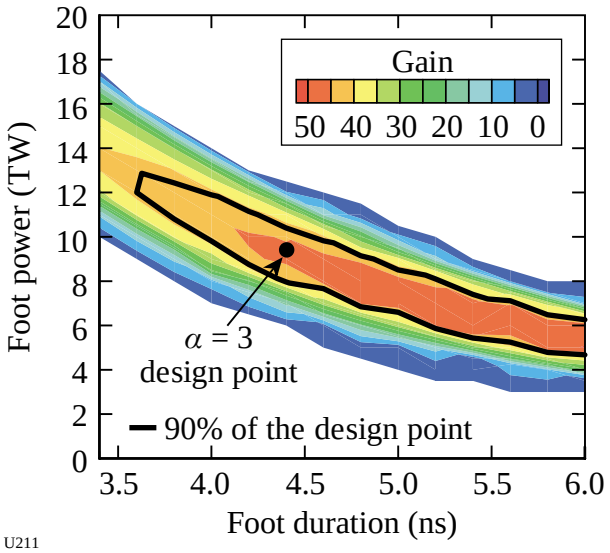

FIG. 3. *Contour plot of equal gain contours, for NIF direct-drive capsule, with foot duration and foot power as the parameters. The black dot indicates the design point.*

3. OMEGA Cryogenic Target Designs

The basis for the OMEGA designs is the NIF direct-drive $\alpha = 3$ design. One-dimensional scaling arguments [5] are used to guide the design of the OMEGA cryogenic targets. The laser energy (E) required to contribute to a given plasma thermal energy scales roughly as the radius of the capsule (R) according to $E \sim R^3$. Since OMEGA delivers 30 kJ of energy, the radius of the OMEGA capsule will be approximately 30% of the NIF design. The corresponding OMEGA laser pulse is determined by noting that the time (t) or duration of the laser pulse scales as the confinement time and is roughly proportional to the radius of the target: $t \sim R$. The scaling of the peak power (P) in the laser pulse can be obtained from the energy and time scaling: $P \sim R^2$. Consequently the length of the laser pulse decreases from 9.25 ns in the NIF design to 2.5 ns for the OMEGA design. The peak power then scales to 32 TW. Processes other than hydrodynamics, such as radiation, thermal transport, and thermonuclear burn, do not scale in a simple manner between the ignition designs and the OMEGA cryogenic designs. These energy-scaled targets possess similar 1-D behavior and instability growth as the ignition designs, thus meeting the requirement of hydrodynamic equivalence.

A series of detailed 1-D simulations were carried out to show that energy-scaled OMEGA cryogenic capsules behave in a similar way to the NIF high-gain optimized capsules. The two-

shock NIF design is compared to a scaled OMEGA capsule in *FIG. 4*. The difference in arrival time for the second shock in the OMEGA design compared to the NIF design is a consequence of lower laser-energy absorption in the OMEGA design. Since the NIF designs typically have scale lengths that are 2 to 3 times longer than OMEGA, the absorption fraction for the NIF ignition designs is 60% while that of OMEGA is only 40%. Table I lists some of the key parameters calculated by 1-D simulations for the two designs. Note that the OMEGA and NIF designs have similar peak shell velocities, hot-spot convergence ratios, and in-flight aspect ratios (IFAR).

Through the use of an instability postprocessor to the 1-D hydrocode *LILAC* [6] both the OMEGA and NIF direct-drive designs are predicted to survive the acceleration phase. The NIF mix width is predicted to be approximately 35% of the overdense shell thickness, whereas the OMEGA mix width will be as much as 85% of the shell thickness. The OMEGA design has a lower safety factor for survival through the acceleration phase than the NIF point design.

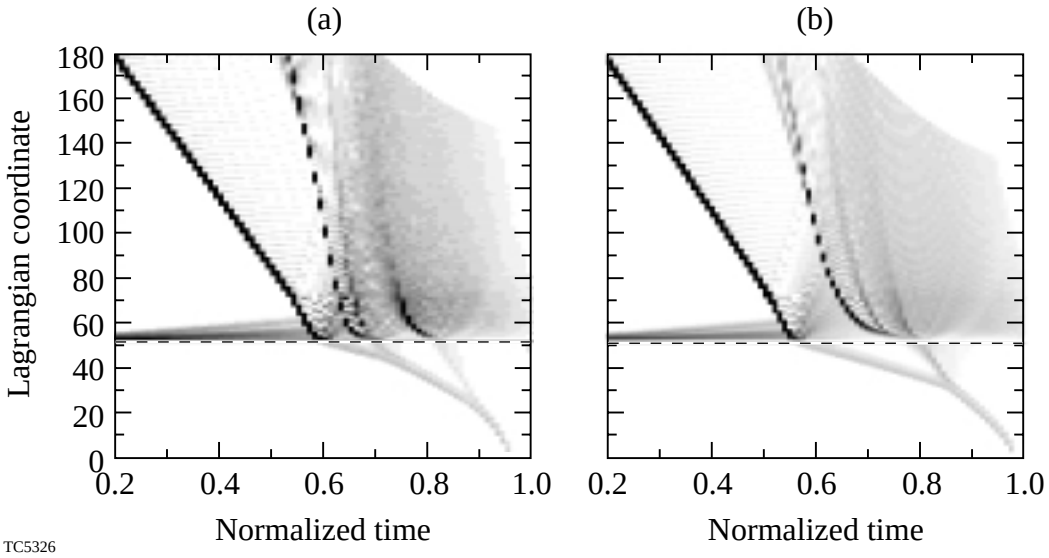

FIG. 4. *Shock propagation as shown by a contour map of the logarithmic derivative of the pressure as a function of normalized time and Lagrangian coordinate for (a) the NIF and (b) the OMEGA designs. Time has been normalized to the incident laser energy, with t = 1.0 corresponding to the end of the laser pulse. This allows the two designs to be compared at the same stage of the implosion. The darker shading indicates a larger pressure gradient and thus captures the position of the shocks. The OMEGA design shows similar timing for the first shock but a delayed second shock compared to the NIF design.*

TAB. I: COMPARISON OF PREDICTED ONE-DIMENSIONAL PARAMETERS BETWEEN THE NIF AND OMEGA CRYOGENIC TARGET DESIGNS.

	NIF	**OMEGA**
Absorption fraction	60%	40%
Hydrodynamic efficiency	11%	12%
Coupling efficiency	7%	4.5%
Peak shell velocity (cm/s)	4.0×10^7	3.7×10^7
Hot-spot convergence ratio	28	20
Peak in-flight aspect ratio	60	50
Peak areal density (mg/cm^2)	1200	300
Neutron-averaged ion temperature (keV)	30	4
Neutron yield	2.5×10^{19}	1.8×10^{14}

The instability postprocessor cannot self-consistently determine the degradation of target yield for a given initial level of nonuniformity. *ORCHID* 2-D hydrocode simulations [4] were used to determine the effect of nonuniformities of inner-ice distortions at the start of the deceleration phase on the overall target performance. These calculations indicate (see *FIG. 5*) that OMEGA cryogenic targets with 1-Thz$_{UV}$, 2-D SSD and 1 μm of inner-ice-surface roughness should obtain approximately 30% of the 1-D yield. Using the same analysis and similar target and laser uniformity levels, we predict that the $\alpha = 3$ direct-drive ignition design will give a gain of 28 on the NIF, a reduction to 60% of the 1-D yield.

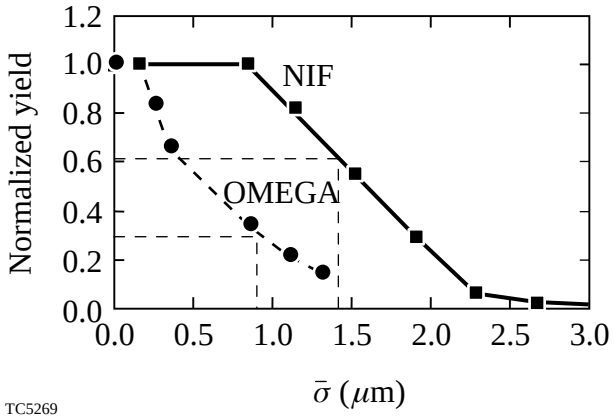

FIG. 5. *Predicted fusion yield (normalized to that of 1-D simulations) for NIF and OMEGA as a function of $\bar{\sigma}$, the effective nonuniformity at the start of the deceleration phase. The dashed lines correspond to the predicted $\bar{\sigma}$ levels for NIF and OMEGA (1.3 μm and 0.9 μm, respectively). OMEGA capsules suffer a larger reduction in yield for a given nonuniformity level than the NIF designs. This can be attributed to the OMEGA design's smaller hot-spot radius compared to that of the NIF point design, which makes the OMEGA hot spot more easily disrupted by the penetration of cold spikes from the main fuel layer.*

4. Irradiation Uniformity

Various techniques, including two-dimensional smoothing by spectral dispersion (2-D SSD) [7–9], distributed phase plates (DPP's) [10,11], polarization smoothing (PS) utilizing distributed polarization rotators (DPR's) [12,13], beam-to-beam precision power balance, and beam overlap, are being used to achieve the high irradiation uniformity required for direct-drive laser-fusion experiments on OMEGA. These techniques will be applicable to the NIF and should be sufficient to reach the rms nonuniformity level of 1% or less when the laser intensity is averaged over a few hundred picoseconds.

FIGURE 6 shows the effects of improvements in the on-target uniformity that have been implemented on OMEGA during the last year. The original SSD configuration consisted of IR bandwidths of 1.25×1.75 Å with electro-optic (EO) modulators of 3 and 3.3 GHz. The spectral divergence was less than 50 μrad. In the last year, one of the modulators was replaced with a 10-GHz modulator, and IR bandwidth was increased to ~12 Å, resulting in a UV bandwidth of ~1 THz. To accommodate the higher bandwidth in frequency tripling, a third frequency-conversion crystal has been added to all the OMEGA frequency-conversion-crystal assemblies [14,15]. In addition, polarization wedges (DPR's) in the form of specially cut KDP crystals have been added to all the OMEGA beamlines.

The current configuration of SSD and PS (bottom curve in *FIG. 6*) results in overall smoothing of the irradiation uniformity to less than 1% rms in less than 300 ps. The total nonuniformity in

the long-wavelength modes (spherical-harmonic modes 11 to 30) can be smoothed to levels below 0.15%.

In addition to the application of individual beam smoothing such as SSD, it is also necessary to control the beam-to-beam power imbalance to levels below ~5% rms. On OMEGA, such control is implemented by the use of precision beam splitting and gain control on all beamlines. Precision calorimeters and high-resolution optical streak cameras that can currently monitor 50 of the 60 OMEGA beams measure the power balance. Extension of this streak camera system to 60 beams is planned in the near future. *FIGURE 7* shows a typical measurement of power balance for 40 of the beams carried out using the OMEGA multibeam streak camera system. Power imbalance of the order of ~5% rms has been demonstrated for 1-ns square pulses.

All of these uniformity improvements are directly applicable to the NIF. As with OMEGA, the current pinhole specification for the NIF limits the angular spread of the beams to 50 μrad. The NIF optical design will need to be examined to determine if the pinholes can be opened farther for direct-drive experiments as was done on OMEGA. A comparison between NIF and OMEGA uniformity is shown in *FIG. 8*. The lower NIF nonuniformity level is due to the larger number of beams on NIF (192) compared to OMEGA (60). It is expected that the NIF smoothing rate and uniformity level should be adequate for direct-drive ignition experiments.

5. LLE's Target Physics Research Program

LLE's target physics research program combines all aspects of direct-drive ICF. Specifically, the program addresses (a) early-time phenomena such as plasma formation, laser–plasma instabilities, laser imprinting, and shock formation; (b) Rayleigh–Taylor growth, mitigation, and saturation in the acceleration phase of the target compression; (c) Rayleigh–Taylor growth

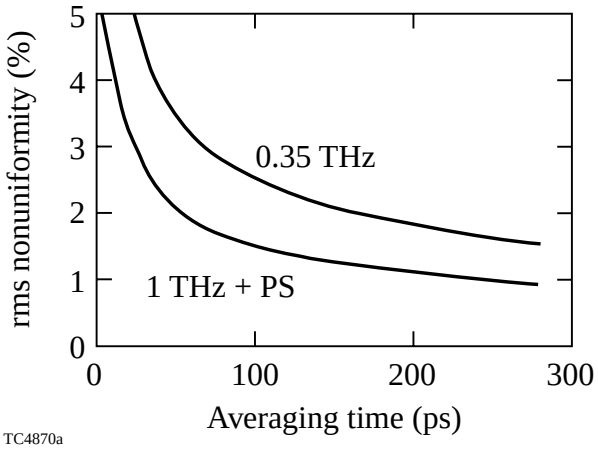

FIG. 6. *The rms nonuniformity as a function of time calculated assuming multiple-beam overlap on a spherical target in the OMEGA 60-beam geometry. Curves are shown for two different configurations of SSD and PS. The current OMEGA configuration includes 1-THz 2-D SSD and PS.*

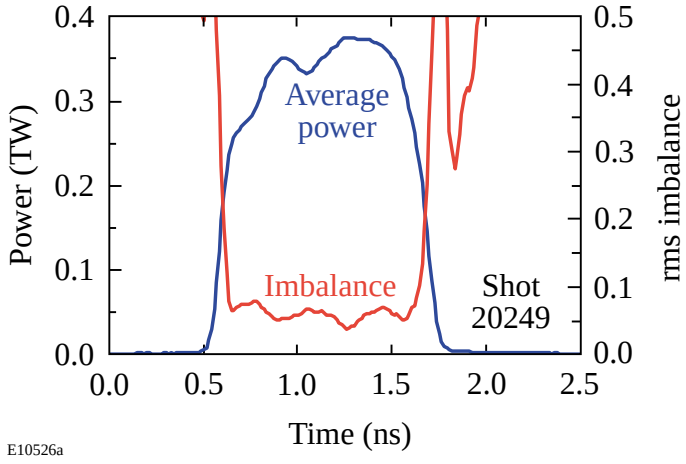

FIG. 7. *Average power and power imbalance as a function of time. These measurements are a 40-beam average with a 1-ns square with 22 kJ on target.*

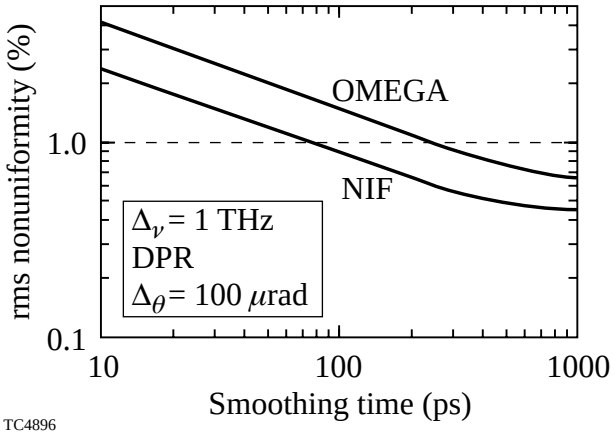

FIG. 8. *The rms nonuniformity is plotted as a function of time for the NIF and for OMEGA, assuming 1-THz bandwidth and polarization smoothing. All spherical-harmonic modes between 5 and 500 are included in the calculation.*

during the deceleration phase; and (d) stagnation and core–shell mixing during peak compression. A variety of plasma diagnostic techniques are applied to study the physics of each of these phases of the target implosion.

The current OMEGA implosion experiments use CH shells that are energy scaled from NIF ignition target designs. *FIGURE 9* schematically compares the typical OMEGA noncryogenic targets to OMEGA cryogenic targets. In the noncryogenic targets, the CH shell corresponds to the main fuel layer (DT ice) and the fill gas corresponds to the hot-spot-forming central DT gas.

The choice of shell thickness for the OMEGA noncryogenic targets is primarily motivated by the fact that 1-mm-diam, 20-μm-thick CH shells driven by 1-ns square pulses have shell stability characteristics similar to the OMEGA $\alpha = 3$ cryogenic target designs (*FIG. 10*).

The goal of the OMEGA noncryogenic target implosions is to study core conditions and mix characteristics. Several target diagnostics and target types are used in these experiments (as shown on Table II).

Several experimental campaigns have been conducted using a single target configuration consisting of a 910- to 930-μm-diam, 18- to 20-μm-thick CH shell filled with 13 to 15 atm of D_2 or DT. These shells have been irradiated with ~23 kJ of UV energy in a 1-ns nearly square pulse. Several beam-smoothing configurations have been used in these experiments including 3-color-cycle, 0.35-THz SSD without PS and 1-color-cycle, 1-THz SSD with PS. The beam-to-beam power balance in the most recent set of experiments has averaged <5% rms (see *FIG. 7*).

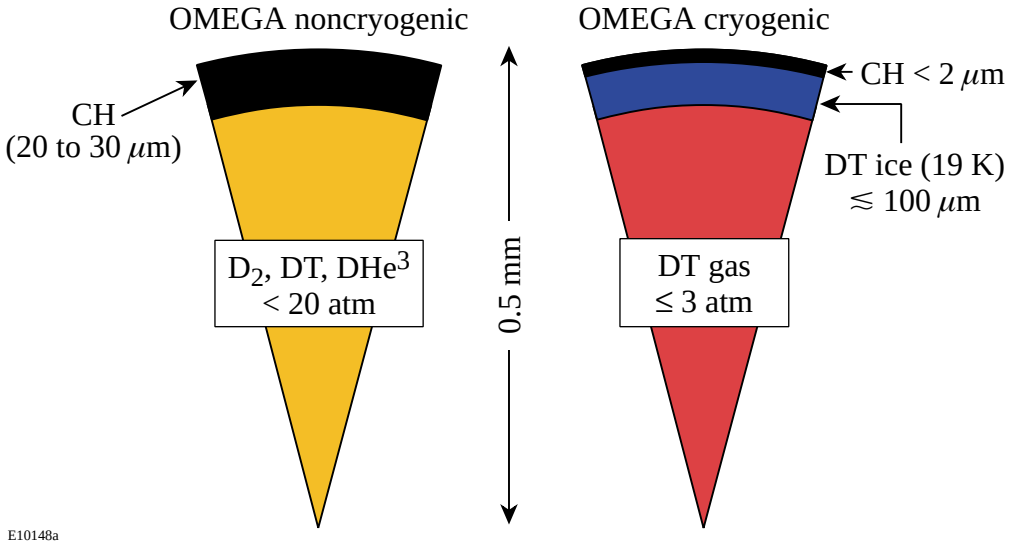

FIG. 9. *Sketch of typical OMEGA noncryogenic (left) and cryogenic implosion targets.*

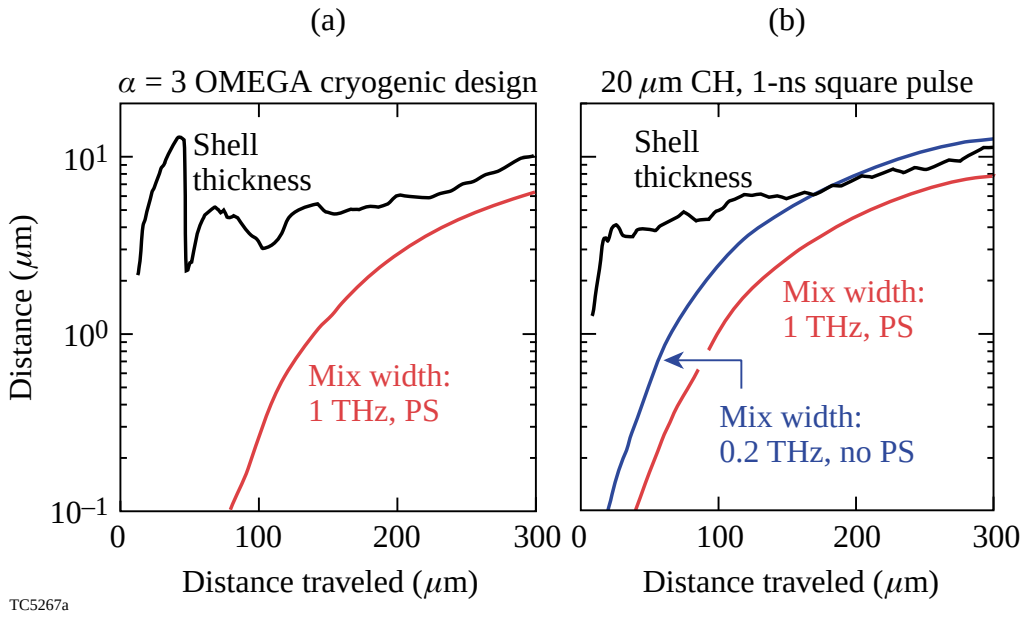

FIG. 10. *Comparison of the characteristic mix width and shell thickness for the OMEGA cryogenic design and the OMEGA warm capsule. The mix width is calculated using an instability model that includes Richtmyer–Meshkov (RM), Rayleigh–Taylor (RT), and Bell–Plesset (BP) instabilities [6] and 3-D Haan saturation [16].*

TAB. II: OMEGA NONCRYOGENIC TARGET IMPLOSION TYPES.

Target Type	Measured Parameters
D_2 and DT-filled CH shells	Primary yield, fuel and shell ρR, T_i, bang time
CH shells with CD layers	Shell conditions and fuel/shell mix
CH shells with CHTi layers	Shell/fuel mix, shell integrity
D_2 with Ar/Kr dopants	Average core fuel electron temperature/density

Several nuclear measurements are made on these compression experiments to assess the fuel conditions at the time of thermonuclear burn. These include primary neutron yield; secondary neutron yield, secondary proton yield, and spectra [17–19] (for D_2-filled targets); neutron-averaged ion temperature; knock-on proton, deuteron, and triton yield and spectra [20, 21] (for DT-filled shells); and burn time history. In addition to neutron diagnostics, a large array of x-ray imaging and spectroscopic diagnostics are also used in these experiments.

Typical charged-particle measurements from experiments with full beam smoothing (1-THz, 2-D SSD with PS), including knock-on deuterons and knock-on protons (from DT-filled capsule implosions) and secondary protons (from a D_2-filled capsule implosion), are shown in *FIG. 11*. The targets were ~920-μm-diam, 19-μm-thick CH shells filled with 15 atm of D_2 or DT and irradiated with 1-ns square pulses with 23 kJ of UV laser light. The top left of *FIG. 11* shows the knock-on deuteron spectrum from shot 20699; this spectrum indicates a fuel areal density of 16 mg/cm^2 (using a uniform ice-block model [18]). At top right is the knock-on proton spectrum (from the CH shell) for shot 20699. This spectrum implies a shell areal density of 61 mg/cm^2. At the bottom of the figure is the integrated secondary proton spectrum from shots 20789, 20790, and 20791. These targets were D_2-filled shells similar in dimension and laser conditions to shot 20699. The secondary protons are produced with energies ranging from 12.5 to 17.5 MeV and are slowed down as they traverse the dense plasma. The total capsule areal density inferred from

this measurement is 76 mg/cm^2—consistent with the total fuel and shell areal density measured on the DT shell of shot 20699. *LILAC* 1-D hydrocode simulations predict a fuel $\rho R \sim 17$ mg/cm^2 and shell $\rho R \sim 64$ mg/cm^2 for these implosions—in good agreement with the experimental measurements. The calculated fuel convergence ratio is ~15. The simulations also predict a primary yield approximately three times larger than measured.

Table III summarizes the comparative performance of these types of targets (with D_2 or DT fills) for implosions with 1-Thz 2-D SSD and PS and those with 3-color-cycle, 0.35-Thz 2-D SSD without PS. Full beam smoothing significantly improves in target performance.

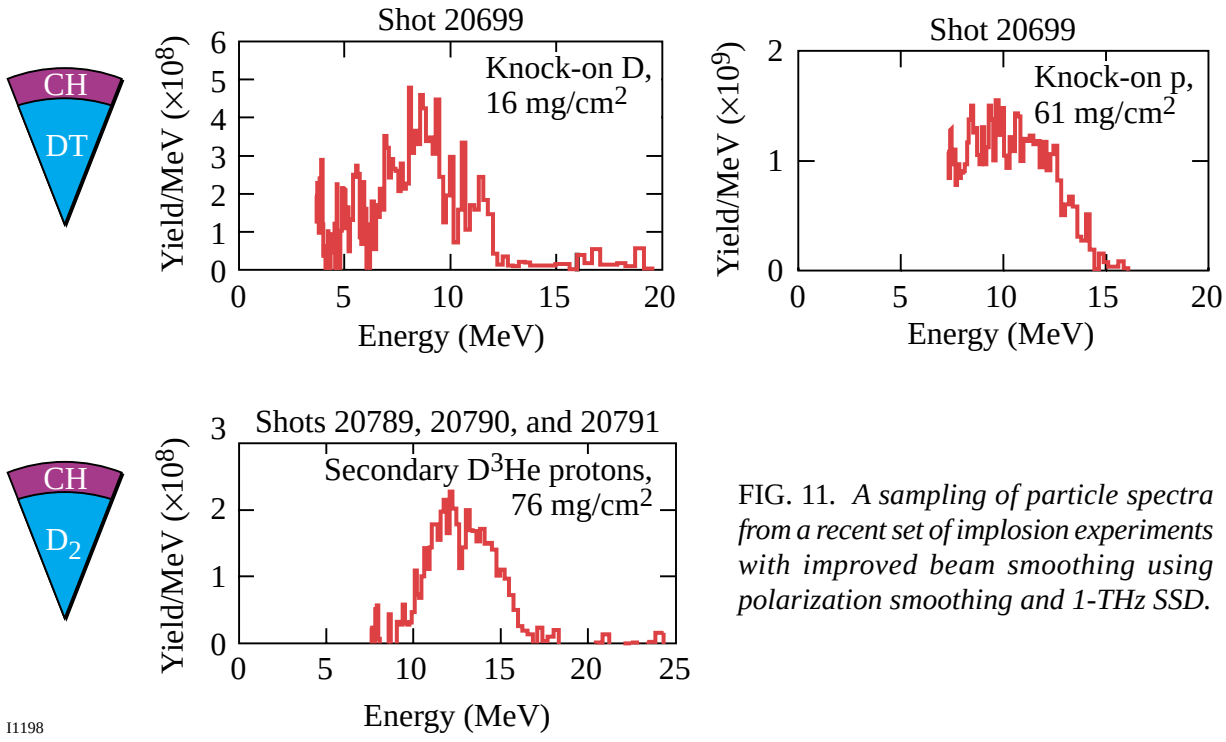

FIG. 11. *A sampling of particle spectra from a recent set of implosion experiments with improved beam smoothing using polarization smoothing and 1-THz SSD.*

TAB. III: SUMMARY OF NUCLEAR MEASUREMENTS ON 19-MM-THICK CH SHELLS FILLED WITH 15 ATM OF D_2 OR DT AND IRRADIATED WITH 1-NS SQUARE PULSES WITH 23 kJ OF UV LASER LIGHT.

Measurement	**3-cycle, 0.35-THz SSD**	**1-cycle, 1-THz SSD, with PS**
D_2 primary yield (10^{10})	9±1	16±1
T_{ion} (D_2)	3.2 keV	3.7 keV
Secondary neutron ratio (10^{-3})	1.5±0.4	2.5±0.2
Secondary proton ratio (10^{-3})	1.4±0.2	1.9±0.2
DT primary yield (10^{12})	6±1	11±3
T_{ion} (DT)	3.7 keV	4.4 keV
Knock-on ratio (10^{-5})	9±3	13±3

6. Cryogenic Targets on OMEGA

The first cryogenic capsule implosion using the OMEGA Cryogenic Target Handling System (CTHS) was carried out on 14 July 2000 (see *FIG. 12*). The primary purpose of this shot was to test the fully integrated CTHS subsystems using a deuterium-filled capsule. The capsule consisted of a 939-μm-diam, 9-μm-thick CD shell filled with deuterium to 1003 atm at 303 K, resulting in a 96-μm-thick ice layer. To minimize the support structure mass and provide a relatively stiff support, the capsule was suspended by three 0.5-μm-thick spider-silk strands in a "C"-shaped Be wire mount.

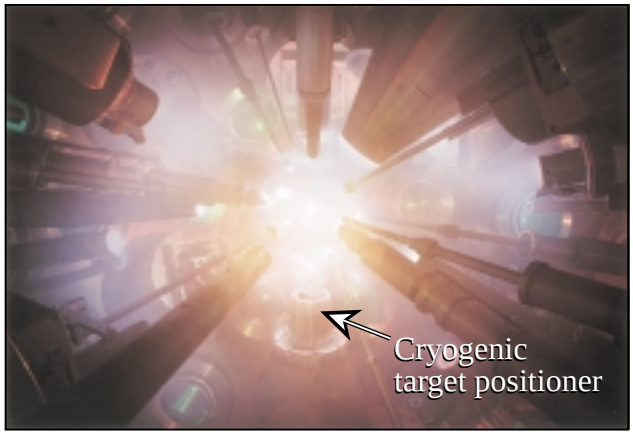

T1554

FIG. 12. *Photograph of the OMEGA target chamber during the first target shot using the CTHS. At the bottom center of the photograph is the cryogenic target positioner.*

The energy on target was 16 kJ in a 1-ns square pulse. For this first test shot, fewer than half of the OMEGA 60 beams were used in order to protect the system from opposing beam damage in the event that the target was not in its prescribed location after shroud retraction. The ice-layer-thickness uniformity was not characterized. The primary DD neutron yield was $3.5\pm0.3 \times 10^8$, and the ion temperature was 5.1±1.3 keV.

This first test shot was the culmination of an intensive activation program, which focused on several issues: characterizing and minimizing target vibration; testing and refining the target manipulation at cryogenic temperatures; and testing the control software for the retraction of the thermal shroud (around the target) and the timing sequence for firing the laser. Issues that require further study are (1) the target vibration induced by the retracting shroud and (2) the production and characterization of a smooth ice layer in a target.

A major source of target vibration is the initial shroud separation. The target has a resonant frequency of 284 Hz at 77 K and vibrates with a maximum amplitude of ~20 μm. During shroud retraction, however, the vibration can exceed ~100 μm. The velocity profile of the shroud retraction was programmed to minimize this vibration (see *FIG. 13*).

7. Summary

LLE is investigating various theoretical aspects of a direct-drive NIF ignition target based on an all-DT design: a spherical target of ~3.4-mm diameter, 1 to 2 μm of CH wall thickness, and an ~350-μm DT-ice layer near the triple point of DT (~19 K). OMEGA experiments are designed to address the critical issues related to direct-drive laser fusion and to provide the necessary data to validate the predictive capability of LLE computer codes. Future cryogenic targets used on OMEGA will be hydrodynamically equivalent to those planned for the NIF. The current experimental studies on OMEGA address the essential components of direct-drive laser fusion: irradiation uniformity and laser imprinting, Rayleigh–Taylor growth and saturation, compressed

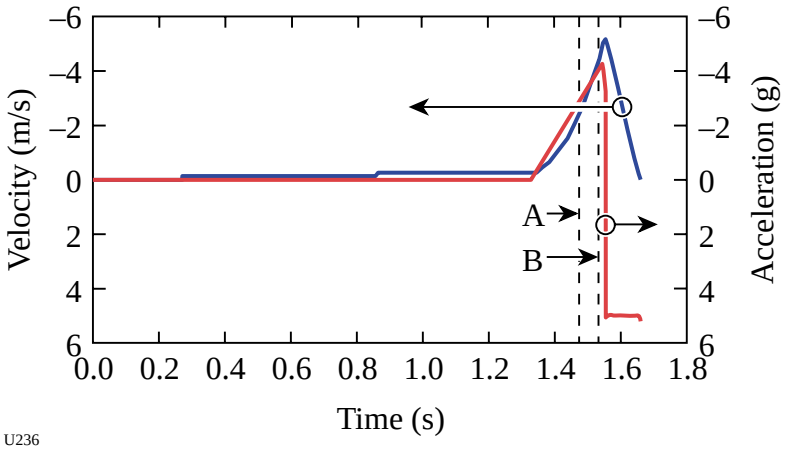

FIG. 13. *The acceleration time history of the shroud retraction is designed to minimize target vibration. The linear motor (LIM) translating the shroud initially accelerates at constant acceleration (–0.023 g) until all the mating surfaces part. The LIM then accelerates to a maximum velocity of 5 m/s followed by a deceleration at 5 g until the system comes to rest. The target is exposed at time A, and the laser fires 54 ms later at point B.*

core performance and shell–fuel mixing, laser–plasma interactions and their effect on target performance, and cryogenic target fabrication and handling. Recent improvements in irradiation uniformity resulted in significant improvements in target performance with fuel and shell ρR in these experiments nearly equal to 1-D hydrocode predictions.

8. Acknowledgment

This work was supported by the U.S. Department of Energy Office of Inertial Confinement Fusion under Cooperative Agreement No. DE-FC03-92SF19460, the University of Rochester, and the New York State Energy Research and Development Authority. The support of DOE does not constitute an endorsement by DOE of the views expressed in this article.

9. References

[1] BODNER, S.E., *et al.*, "Direct-drive laser fusion: Status and prospects," Phys. Plasmas **5** (1998) 1901–1918.

[2] LINDL, J.D., "Development of the indirect-drive approach to inertial confinement fusion and the target physics basis for ignition and gain," Phys. Plasmas **2** (1995) 3933–4024.

[3] BOEHLY, T.R., *et al.*, "Initial performance results of the OMEGA laser system," Opt. Commun. **133** (1997) 495-506; SOURES, J.M., *et al.*, "Direct-drive laser-fusion experiments with the OMEGA, 60-beam, >40-kJ, ultraviolet laser system," Phys. Plasmas **3** (1996) 2108–2112.

[4] "OMEGA cryogenic target designs," Laboratory for Laser Energetics LLE Review **82**, 49–55, NTIS document No. DOE/SF/19460-344 (2000); "Direct-drive target designs for the National Ignition Facility," Laboratory for Laser Energetics LLE Review **79**, 121–130, NTIS document No. DOE/SF/19460-317 (1999). Copies may be obtained from the National Technical Information Service, Springfield, VA 22161.

[5] BRUECKNER, K.A., JORNA, S., "Laser-driven fusion," Rev. Mod. Phys. **46** (1974) 325–367.

[6] GONCHAROV, V.N., "Self-consistent stability analysis of ablation fronts in inertial confinement fusion," Ph.D thesis, University of Rochester (1998); GONCHAROV, V.N., *et al.*, "Modeling hydrodynamic instabilities in inertial confinement fusion targets,"

accepted for publication in Phys. Plasmas; "Stability analysis of directly driven NIF capsules," Laboratory for Laser Energetics LLE Review **81**, 1-5, NTIS document No. DOE/SF/19460-335 (1999). Copies may be obtained from the National Technical Information Service, Springfield, VA 22161.

[7] SKUPSKY, S., *et al.*, "Improved laser-beam uniformity using the angular dispersion of frequency-modulated light," J. Appl. Phys. **66** (1989) 3456–3462.

[8] SKUPSKY, S., CRAXTON, R.S., "Irradiation uniformity for high-compression laser-fusion experiments," Phys. Plasmas **6** (1999) 2157–2163; "Two-dimensional SSD on OMEGA," Laboratory for Laser Energetics LLE Review **69**, 1-10, NTIS document No. DOE/SF/19460–152 (1996). Copies may be obtained from the National Technical Information Service, Springfield, VA 22161.

[9] ROTHENBERG, J.E., "Comparison of beam-smoothing methods for direct-drive inertial confinement fusion," J. Opt. Soc. Am. B **14** (1997) 1664–1671.

[10] KESSLER, T.J., *et al.*, "Phase conversion of lasers with low-loss distributed phase plates," in *Laser Coherence Control: Technology and Applications*, POWELL, H.T., KESSLER, T.J. (Eds.), SPIE, Bellingham, WA (1993), Vol. 1870, pp. 95–104.

[11] LIN, Y., KESSLER, T.J., LAWRENCE, G.N., "Design of continuous surface-relief phase plates by surface-based simulated annealing to achieve control of focal-plane irradiance," Opt. Lett. **21** (1996) 1703–1705.

[12] TSUBAKIMOTO, K., *et al.*, "Suppression of interference speckles produced by a random phase plate, using a polarization control plate," Opt. Commun. **91** (1992) 9–12.

[13] GUNDERMAN, T.E., *et al.*, "Liquid crystal distributed polarization rotator for improved uniformity of focused laser light," in *Conference on Lasers and Electro-Optics* Vol. 7, 1990 OSA Technical Digest Series, Optical Society of America, Washington, DC (1990), p. 354.

[14] EIMERL, D., *et al.*, "Multicrystal designs for efficient third-harmonic generation," Opt. Lett. **22** (1997) 1208–1210.

[15] BABUSHKIN, A., *et al.*, "Demonstration of the dual-tripler scheme for increased-bandwidth third-harmonic generation," Opt. Lett. **23** (1998) 927–929.

[16] HAAN, S.W., "Onset of nonlinear saturation for Rayleigh-Taylor growth in the presence of a full spectrum of modes," Phys. Rev. A **39** (1989) 5812–5825.

[17] GLEBOV, V.YU., *et al.*, "Secondary-neutron-yield measurements by current-mode detectors," to be published in Rev. Sci. Instrum.

[18] LI, C.K., *et al.*, "D^3He proton spectra for diagnosing shell ρR and fuel T_i of imploded capsules at OMEGA," Phys. Plasmas **7** (2000) 2578–2584.

[19] SEGUIN, F., *et al.*, "Using secondary proton spectra to study imploded D_2-filled capsules at the OMEGA laser facility," to be submitted for publication.

[20] RADHA, P.B., *et al.*, "A novel charged-particle diagnostic for compression in inertial confinement fusion targets," Phys. Plasmas **7** (2000) 1531–1538.

[21] LI, C.K., *et al*., "Study of direct-drive, DT gas-filled plastic capsule implosions using nuclear diagnostics at OMEGA," to be published.